Supplementary Material

Supplementary Analysis: Models S1

For comparability with the 200 s long fNIRS measurements during metronomic breathing, the main analyses included also only the first 200 s of the 15 min resting state measurements. To assure the time-invariance of the resting-state connectivity (across the overall 15 min measurement) we performed a control analysis of four consecutive, 200 s long segments of the resting state data and fitted a linear mixed model with the fixed effects structure comprising the 3-way interaction between *direction*, *time window* and *hemisphere* (including all main effects and lower-order interactions, Supplementary Table S3). Identical to all other mixed models in the present study, the random effects were specified with a random slope allowing for varying effects of *direction* for each pair of homologues connections and a random intercept for *participant* (Supplementary Table S2). The model yielded two significant effects: a main effect for *direction* ($F(1,12) = 12.9$, $p = .004$) and an interaction between *direction* and *hemisphere* ($F(1,2460) = 4.9$, $p = .027$). Predicted marginal means and statistics for all fixed effects are provided in Supplementary Table S1 and S3, respectively. As the factor *time window* did not exert any significant main or interaction effect, the present results hence do not depend on the chosen segment of the resting state measurements.

Supplementary Analysis: Models S2-S5

FNIRS measurements are prone to motion-induced artifacts that can bias estimates of functional connectivity and applying an appropriate correction method is strongly advised (Satterthwaite et al. 2012; Santosa et al. 2017). However, the correlation based signal improvement (CBSI) method, used in the present analyses to remove motion artifacts, is based on assumptions that are not always met (Cui et al. 2010) and to the best of our knowledge, a systematic investigation of the impact of the CBSI method on Granger causality inference has not been published yet. We therefore complemented the main analyses in Model 1 (DC estimates without covariate) and Model 2 (PDC estimates including aBP as a covariate) by estimating DC and PDC from the uncorrected data of deoxygenated (Models S2

[DC] and S4 [PDC]) and oxygenated (Models S3 [DC] and S5 [PDC]) hemoglobin concentration changes. Estimates for significant effects and statistics for random and fixed effects are summarized in Supplementary Table S1, S2 and S3, respectively. Bar graphs in Supplementary Figure S1 (Model S2 and S3) and Figure S2 (Model S4 and S5) show the connectivity estimates analogue to Figure 3 (Model 1) and Figure 4 (Model 2) in the main text, respectively.

Supplementary Model S2 analyzed the DC estimated from the deoxygenated hemoglobin (dxyHb) data and yielded a significant main effect for *direction* ($F(1,12) = 11.1$, $p = .006$) and for *condition* ($F(1,1223) = 28.6$, $p < .0001$). Model S3 analyzed the oxygenated hemoglobin (oxyHb) data and yielded a main effect for *condition* ($F(1,1212) = 76.0$, $p < .0001$) only. Neither the interaction between *direction* and *hemisphere*, nor the interaction between *direction*, *condition* and *hemisphere* (that were significant in Model 1 using the CBSI data) were significant for the data not corrected for motion artifacts. However, the overall pattern of connectivity estimated from the dxyHb data was highly similar to those estimated from the CBSI data (Figure S1), while the pattern for the oxyHb data revealed an obvious deviation when compared to the CBSI data. Importantly, this deviation was markedly reduced for the PDC estimates that were corrected for influences by systemic aBP fluctuations, for both the dxyHb and the oxyHb data: Supplementary Model S4 analyzed the PDC (corrected for aPB influences) estimated from the dxyHb data and revealed a significant main effect for *direction* ($F(1,12) = 11.6$, $p = .005$); Model S5 analyzed the PDC estimated from the oxyHb data and revealed a significant main effect for *direction* ($F(1,12) = 13.7$, $p = .003$) and for the interaction between *direction* and *hemisphere* ($F(1,1212) = 8.4$, $p = .004$). Thus, similar to the main analyses of the CBSI data, correcting the connectivity for influences by aBP fluctuations removed the effects of *condition* in the dxyHb and the oxyHb data; at the same time the difference between healthy and affected hemispheres resembled the results from the CBSI data.

The deviating pattern in the DC values estimated from the oxyHb data is most likely due to the fact that the oxyHb signal contains more physiological noise than the dxyHb signal (Obrig et al. 2000; Zhang et al. 2009; Kirilina et al. 2012; Sutoko et al. 2019) and the observation that correcting for aBP influences brought the results from the dxyHb, oxyHb and the CBSI data into line, corroborates our

finding that aBP-PDC effectively controls for bias of the functional connectivity estimate induced by physiological noise.

Supplementary Figure S1

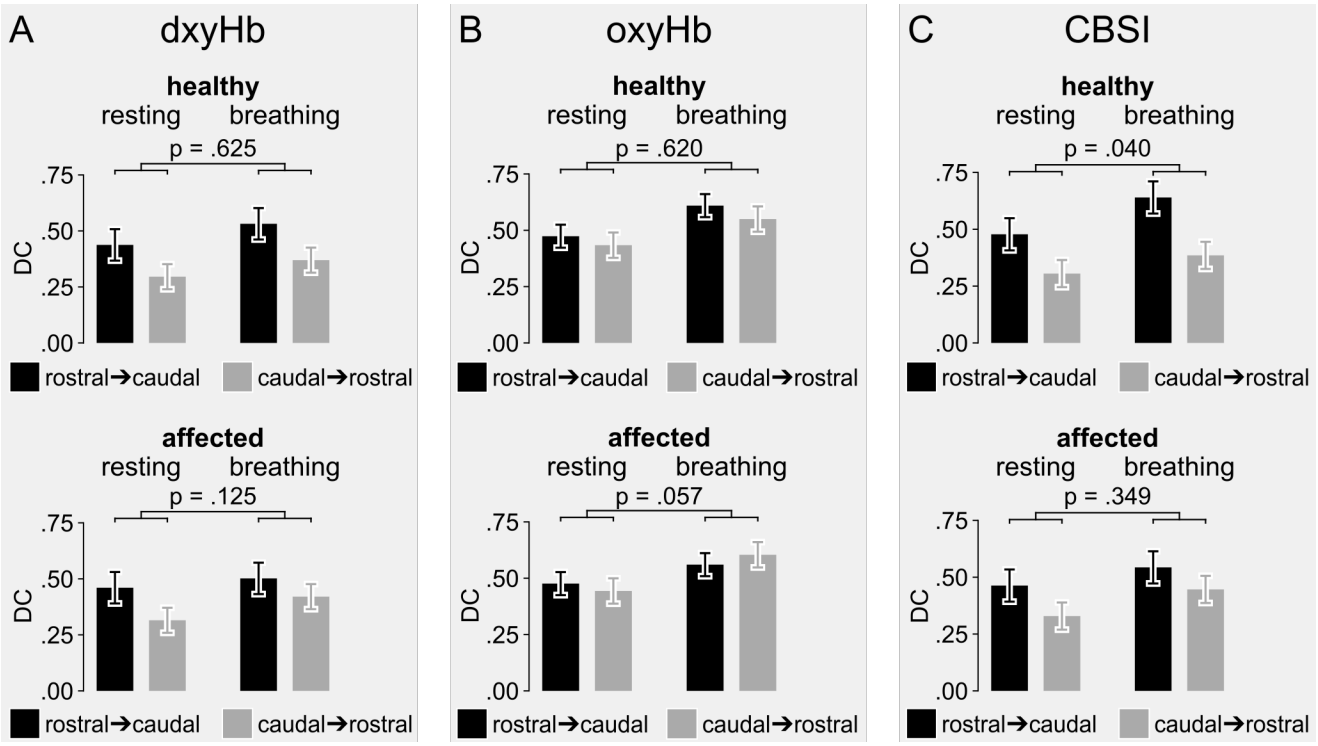

Supplementary Figure S1: Comparison of DC estimates without applying an artifact correction to the DC derived from the data preprocessed using the correlation based signal improvement (CBSI). The connectivity estimated from the deoxygenated hemoglobin signal (A; Model S2) was similar to the connectivity estimated from the artifact corrected signal (C; Model 1), while the pattern of DC estimates derived from the oxygenated hemoglobin data (B; Model S3) markedly deviated from those derived from the CBSI data.

Supplementary Figure S2

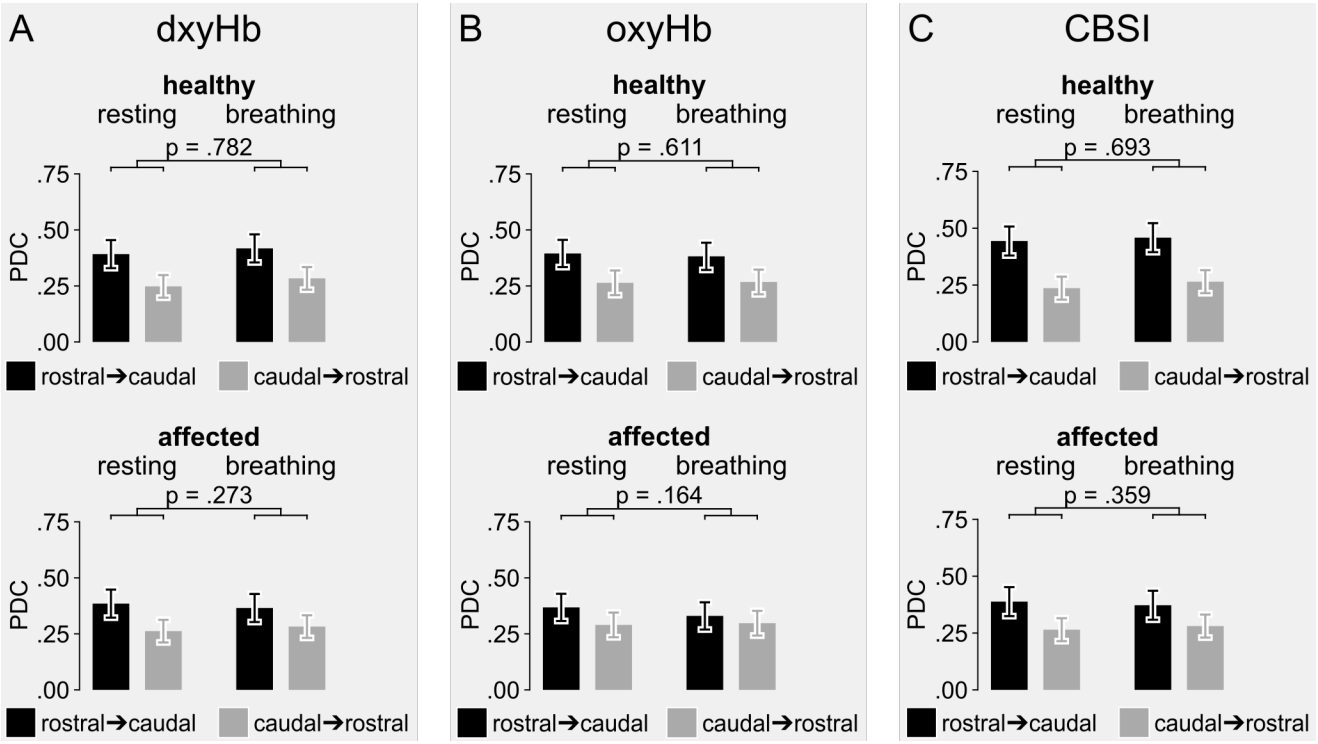

Supplementary Figure S2: Comparison of PDC estimates corrected for aBP fluctuations with and without applying artifact correction (CBSI) during preprocessing. The pattern of PDC estimates were similar for the deoxygenated (A; Model S4), oxygenated (B; Model S5) and CBSI (C, Model 2) data suggesting that the deviating results for the oxyHb-derived DC estimates were due to the higher susceptibility of the oxyHb measurement to physiological noise (Obrig et al. 2000; Zhang et al. 2009; Kirilina et al. 2012; Sutoko et al. 2019) and corroborating our finding, that including the aBP signal in PDC estimation effectively controlled for bias induced by physiological noise.

Supplementary Analysis: Model S6

In order to explicitly test the effect of correcting the DC connectivity estimates by including the aBP time series in the VAR model, we tested the factors *direction*, *condition*, and *VAR model type* (with and without aBP-correction) and all resulting two- and three-way interactions as fixed effects terms in a linear mixed model (Model S6; with the same random effects structure as in Model 1 and 2; see Supplementary Table S3 for an overview of all fixed effects). This model considered only the healthy hemisphere, because the difference between conditions (resting state vs. breathing) in the uncorrected data was not present in the affected hemisphere. While there was a marked difference between conditions in the uncorrected data (Fig. 3, healthy hemisphere), directed connectivity was almost

identical across conditions in the connectivity estimates corrected for aBP oscillations (Fig. 4, healthy hemisphere); the respective three-way interaction between *direction*, *condition* and *VAR model type* failed to reach significance, though ($F(1,1212) = 3.1$, $p = .077$). Similarly, the significant interaction between *condition* and *VAR model type* ($F(1,1212) = 13.6$, $p = .0002$) and the respective post-hoc comparisons demonstrated, that the increase in overall connectivity strength induced by metronomic breathing was absent after intra-individually adjusting for aBP oscillations. Accordingly, the main effect for *VAR model type* showed that connectivity was attenuated by including aBP in the VAR model ($F(1,1212) = 56.2$, $p < .0001$). Main effects for *direction* ($F(1,12) = 36.8$, $p < .0001$) and *condition* ($F(1,1212) = 28.0$, $p < .0001$) again showed that connectivity in rostro-caudal direction and during metronomic breathing was stronger than in caudo-rostral direction and during resting-state, respectively. No further effects were significant (all $p > .206$).

Supplementary Analysis: Model S7

For the sake of completeness, we also fitted this model to the data of the affected hemisphere (Model S7; see Supplementary Table S3 for an overview of all fixed effects). As indicated by Figures 3 and 4 (affected hemisphere), the three-way interaction between *direction*, *condition* and *VAR model type* was not significant ($F(1,1223) = 0.01$, $p = .914$), i.e. correcting for aBP oscillations had no effect on the condition independent rostro-caudal gradient in the affected hemisphere. Similar as in the healthy hemisphere, the significant interaction between *condition* and *VAR model type* ($F(1,1223) = 14.4$, $p = .0002$) revealed that the increase in overall connectivity strength induced by metronomic breathing disappeared after intra-individually adjusting for aBP oscillations. Again, the main effect for *VAR model type* showed that connectivity was attenuated by including aBP in the VAR model ($F(1,1223) = 83.6$, $p < .0001$). Main effects for *direction* ($F(1,12) = 6.1$, $p = .029$) and *condition* ($F(1,1223) = 14.3$, $p = .0002$) again showed that connectivity in rostro-caudal direction and during metronomic breathing was stronger than in caudo-rostral direction and during resting-state, respectively. No further effects were significant (all $p > .186$).

104 **Supplementary Table S1: Predicted marginal means for significant effects**

105 **in the linear mixed models**

Model (Figures)	Effect	Factor Level			Estimate [SE]	Lower CL	Upper CL
Model 1 DC LMM (Figure 3)	direction	rost.→caud.			.53 [.03]	.47	.59
		caud.→rost.			.37 [.02]	.32	.42
	condition	resting			.39 [.02]	.36	.43
		breathing			.50 [.02]	.47	.54
	direction × condition × hemisphere	rost.→caud.	resting	healthy	.48 [.03]	.41	.55
				affected	.46 [.03]	.39	.53
			breathing	healthy	.64 [.03]	.57	.71
				affected	.54 [.03]	.47	.61
		caud.→rost.	resting	healthy	.30 [.03]	.25	.36
				affected	.33 [.03]	.27	.39
			breathing	healthy	.39 [.03]	.33	.44
				affected	.45 [.03]	.39	.51
Model 2 PDC LMM (aBP corrected connectivity; Figure 4)	direction	rost.→caud.			.42 [.03]	.36	.47
		caud.→rost.			.26 [.02]	.22	.30
	hemisphere	healthy			.35 [.02]	.31	.39
		affected			.33 [.02]	.29	.36
	direction × hemisphere	rost.→caud.	healthy		.45 [.03]	.39	.51
			affected		.38 [.03]	.32	.44
		caud.→rost.	healthy		.25 [.02]	.21	.30
			affected		.27 [.02]	.23	.32
Model 4 DC LMM with fNIRS PSD covariate (Figure 7)	direction	rost.→caud.			.53 [.03]	.46	.59
		caud.→rost.			.37 [.02]	.32	.42
	condition	resting			.40 [.02]	.37	.43
		breathing			.50 [.02]	.46	.53
	PSD_{fNIRS}				.005 [.002]	.001	.009
	direction × hemisphere × PSD_{fNIRS}	rost.→caud.	healthy		.013 [.004]	.005	.020
			affected		.002 [.003]	-.005	.009
		caud.→rost.	healthy		-.002 [.004]	-.009	.006
			affected		.007 [.003]	.001	.014
Model S1 DC LMM (resting state time windows)	direction	rost.→caud.			.48 [.03]	.42	.55
		caud.→rost.			.32 [.02]	.27	.37
	direction × hemisphere	rost.→caud.	healthy		.49 [.03]	.42	.55
			affected		.47 [.03]	.41	.54
		caud.→rost.	healthy		.31 [.02]	.26	.36
			affected		.33 [.02]	.28	.38
Model S2 DC LMM (dxyHb; Figure S1)	direction	rost.→caud.			.48 [.03]	.42	.54
		caud.→rost.			.35 [.02]	.31	.39
	condition	resting			.38 [.02]	.34	.41
		breathing			.46 [.02]	.42	.49
Model S3 DC LMM (oxyHb; Figure S1)	condition	resting			.46 [.02]	.42	.49
		breathing			.58 [.02]	.54	.62
Model S4	direction	rost.→caud.			.39 [.03]	.33	.45

Model (Figures)	Effect	Factor Level		Estimate [SE]	Lower CL	Upper CL
PDC LMM (dxyHb; Figure S2)		caud.→rost.		.27 [.02]	.23	.31
Model S5 PDC LMM (oxyHb; Figure S2)	direction	rost.→caud.		.37 [.03]	.31	.42
		caud.→rost.		.28 [.02]	.23	.33
	direction × hemisphere	rost.→caud.	healthy	.39 [.03]	.33	.45
			affected	.35 [.03]	.29	.41
		caud.→rost.	healthy	.27 [.02]	.22	.32
			affected	.29 [.02]	.24	.34
Model S6 DC vs. PDC LMM (healthy hemisphere; Figure 4 vs Figure 5)	direction	rost.→caud.		.50 [.03]	.45	.56
		caud.→rost.		.30 [.02]	.26	.34
	condition	resting		.37 [.02]	.33	.40
		breathing		.44 [.02]	.40	.47
	VAR model type	DC		.45 [.02]	.42	.49
		PDC		.35 [.02]	.32	.39
	condition × VAR model type	resting	DC	.39 [.02]	.35	.43
			PDC	.34 [.02]	.30	.38
		breathing	DC	.51 [.02]	.47	.55
			PDC	.36 [.02]	.32	.40
Model S7 DC vs. PDC LMM (affected hemisphere; Figure 4 vs Figure 5)	direction	rost.→caud.		.44 [.03]	.38	.50
		caud.→rost.		.33 [.02]	.28	.38
	condition	resting		.36 [.02]	.33	.39
		breathing		.41 [.02]	.38	.44
	VAR model type	DC		.45 [.02]	.41	.48
		PDC		.33 [.02]	.30	.36
	condition × VAR model type	resting	DC	.40 [.02]	.36	.43
			PDC	.33 [.02]	.29	.36
		breathing	DC	.49 [.02]	.46	.53
			PDC	.33 [.02]	.29	.36

NB: Estimates and confidence limits were obtained using the lsmeans package (Lenth 2016) with Satterthwaite approximation of degrees of freedom. For effects involving the continuous predictor PSD_{fNIRS} (underlined) the estimates represent its slopes, while for effects only involving discrete predictors the estimates refer to the predicted marginal means on the given factor level. Abbreviations: caud., caudal; CL, confidence limits; DC, directed coherence; LMM, linear mixed model; PDC, partial directed coherence; PSD_{fNIRS}, power spectral density of the fNIRS signal; rost., rostral; SE, standard error; VAR, vector autoregressive.

113 # Supplementary Table S2: Random effects for linear mixed models

Model	Factor	Type	Variance
Model 1 DC LMM	participant	intercept	.0024
	connection	intercept	.0074
		slope for direction	.0200
	residual		.0617
Model 2 PDC LMM (aBP corrected connectivity)	participant	intercept	.0027
	connection	intercept	.0057
		slope for direction	.0126
	residual		.0465
Model 4 DC LMM with fNIRS PSD covariate	participant	intercept	.0013
	connection	intercept	.0074
		slope for direction	.0200
	residual		.0612
Model S1 DC LMM (resting state time windows)	participant	intercept	.0022
	connection	intercept	.0089
		slope for direction	.0231
	residual		.0557
Model S2 DC LMM (dxyHb)	participant	intercept	.0021
	connection	intercept	.0071
		slope for direction	.0165
	residual		.0677
Model S3 DC LMM (oxyHb)	participant	intercept	.0018
	connection	intercept	.0014
		slope for direction	.0051
	residual		.0632
Model S4 PDC LMM (dxyHb)	participant	intercept	.0020
	connection	intercept	.0056
		slope for direction	.0132
	residual		.0515
Model S5 PDC LMM (oxyHb)	participant	intercept	.0052
	connection	intercept	.0027
		slope for direction	.0053
	residual		.0419
Model S6 DC vs. PDC LMM (healthy hemisphere)	participant	intercept	.0016
	connection	intercept	.0055
		slope for direction	.0118
	residual		.0567
Model S7 DC vs. PDC LMM (affected hemisphere)	participant	intercept	.0016
	connection	intercept	.0079
		slope for direction	.0223
	residual		.0529

114

115 # Supplementary Table S3: Type III statistics for supplementary models

Model (Figures)	Effect	df	Error df	F value	p value
Model S1 DC LMM (resting state time windows)	direction	1	12	12.90	**.0037**
	time window	3	2460	1.09	.3513
	hemisphere	1	2460	.44	.5053
	direction × time window	3	2460	.48	.6961
	direction × hemisphere	1	2460	4.89	**.0272**
	time window × hemisphere	3	2460	.01	.9995
	direction × time window × hemisphere	3	2460	.11	.9559
Model S2 DC LMM (dxyHb; Figure S1)	direction	1	12	11.07	**.0060**
	condition	1	1223	28.63	**1×10^{-7}**
	hemisphere	1	1223	1.17	.2806
	direction × condition	1	1223	.55	.4602
	direction × hemisphere	1	1223	1.73	.1881
	condition × hemisphere	1	1223	.13	.7228
	direction × condition × hemisphere	1	1223	2.04	.1531
Model S3 DC LMM (oxyHb; Figure S1)	direction	1	12	.78	.3943
	condition	1	1212	76.02	**$< 10^{-15}$**
	hemisphere	1	1212	.09	.7590
	direction × condition	1	1212	.99	.3205
	direction × hemisphere	1	1212	3.77	.0525
	condition × hemisphere	1	1212	.02	.9037
	direction × condition × hemisphere	1	1212	2.87	.0903
Model S4 PDC LMM (aBP corrected connectivity; dxyHb; Figure S2)	direction	1	12	11.55	**.0053**
	condition	1	1223	1.46	.2274
	hemisphere	1	1223	.81	.3677
	direction × condition	1	1223	.94	.3312
	direction × hemisphere	1	1223	1.97	.1607
	condition × hemisphere	1	1223	1.39	.2387
	direction × condition × hemisphere	1	1223	.34	.5620
Model S5 PDC LMM (aBP corrected connectivity; oxyHb; Figure S2)	direction	1	12	13.74	**.0030**
	condition	1	1212	.72	.3974
	hemisphere	1	1212	.24	.6246
	direction × condition	1	1212	1.81	.1789
	direction × hemisphere	1	1212	8.42	**.0038**
	condition × hemisphere	1	1212	.21	.6438
	direction × condition × hemisphere	1	1212	.39	.5318
Model S6 DC vs. PDC LMM (healthy hemisphere; Figure 4 vs Figure 5)	direction	1	12	36.83	**.0001**
	condition	1	1212	28.02	**1×10^{-7}**
	VAR model type (DC vs. PDC)	1	1212	56.19	**1×10^{-13}**
	direction × condition	1	1212	1.60	.2064
	direction × VAR model type	1	1212	.24	.6215
	condition × VAR model type	1	1212	13.60	**.0002**
	direction × condition × VAR model type	1	1212	3.13	.0770
Model S7 DC vs. PDC LMM (affected hemisphere; Figure 4 vs Figure 5)	direction	1	12	6.13	**.0291**
	condition	1	1223	14.32	**.0002**
	VAR model type (DC vs. PDC)	1	1223	83.64	**$< 10^{-15}$**
	direction × condition	1	1223	1.75	.1856

Model (Figures)	Effect	df	Error df	F value	p value
	direction × VAR model type	1	1223	.09	.7588
	condition × VAR model type	1	1223	14.36	**.0002**
	direction × condition × VAR model type	1	1223	.01	.9141

NB: Tests of linear mixed models (LMM) were performed using the lmerTest package (Kuznetsova et al. 2016), with Satterthwaite approximation of degrees of freedom. Abbreviations: DC, directed coherence; df, degrees of freedom; LMM, linear mixed model; PDC, partial directed coherence; VAR, vector autoregressive.

References

Cui X, Bray S, Reiss AL (2010) Functional near infrared spectroscopy (NIRS) signal improvement based on negative correlation between oxygenated and deoxygenated hemoglobin dynamics. Neuroimage 49:3039–46. doi: 10.1016/j.neuroimage.2009.11.050

Kirilina E, Jelzow A, Heine A, et al (2012) The physiological origin of task-evoked systemic artefacts in functional near infrared spectroscopy. Neuroimage 61:70–81. doi: 10.1016/j.neuroimage.2012.02.074

Kuznetsova A, Bruun Brockhoff P, Haubo Bojesen Christensen R (2016) lmerTest: Tests in Linear Mixed Effects Models

Lenth R V (2016) Least-Squares Means: The R Package lsmeans. J Stat Softw 69:1–33. doi: 10.18637/jss.v069.i01

Obrig H, Neufang M, Wenzel R, et al (2000) Spontaneous low frequency oscillations of cerebral hemodynamics and metabolism in human adults. Neuroimage 12:623–39. doi: 10.1006/nimg.2000.0657

Santosa H, Aarabi A, Perlman SB, Huppert TJ (2017) Characterization and correction of the false-discovery rates in resting state connectivity using functional near-infrared spectroscopy. J Biomed Opt 22:55002. doi: 10.1117/1.JBO.22.5.055002

Satterthwaite TD, Wolf DH, Loughead J, et al (2012) Impact of in-scanner head motion on multiple measures of functional connectivity: relevance for studies of neurodevelopment in youth. Neuroimage 60:623–32. doi: 10.1016/j.neuroimage.2011.12.063

Sutoko S, Chan YL, Obata A, et al (2019) Denoising of neuronal signal from mixed systemic low-frequency oscillation using peripheral measurement as noise regressor in near-infrared imaging. Neurophotonics 6:015001. doi: 10.1117/1.NPh.6.1.015001

Zhang Q, Strangman GE, Ganis G (2009) Adaptive filtering to reduce global interference in non-invasive NIRS measures of brain activation: How well and when does it work? Neuroimage

145 45:788–794. doi: 10.1016/j.neuroimage.2008.12.048

146